Electronic Supplementary Material (ESI) for New Journal of Chemistry.
This journal is © The Royal Society of Chemistry and the Centre National de la Recherche Scientifique 2021

Supporting Information for

Flexible Modulation of Porous Structure Enables Its Durability as A Sulfur Carrier in Advanced Lithium–Sulfur Batteries

Chen Liu,[a] Fanrong Kong,[b] Jianchao Liu,[a] Ruhong Li,[a] Hongda Zhang,[b] Lin Li,[b] Zhen Wang,[c] Weihua Wan,[c] Junhua Wei,*[c] Changsong Dai*[a]

[a] *MIIT Key Laboratory of Critical Materials Technology for New Energy Conversion and Storage, School of Chemistry and Chemical Engineering, Harbin Institute of Technology, Harbin, 150001, China*
[b] *Electric Power Research Institute, State Grid Heilongjiang Electric Power Co., Ltd., Harbin, 150030, China*
[c] *State Key Laboratory of Advanced Chemical Power Sources, Guizhou Meiling Power Sources Co., Ltd., Zunyi, 563003, China*

Table S1. Factor/level comparison.

LEVEL	FACTOR		
	A Hydrothermal temperature (℃)	B Processing time (h)	C Carbon black raw material
1	140	0.25	KB-q(Ketjen Black, EC600JD)
2	150	0.5	KB-f(Ketjen Black, ECP600JD)
3	160	1.0	SP(Super P)
4	170	1.5	AB(Acetylene black)

Table S2. Standard orthogonal table for experiment.

NUMBER	FACTOR		
	A Hydrothermal temperature(℃)	B Processing time(h)	C Carbon black raw material
1	1	1	1
2	1	2	2
3	1	3	3
4	1	4	4
5	2	1	2
6	2	2	1
7	2	3	4
8	2	4	3
9	3	1	3
10	3	2	4
11	3	3	1
12	3	4	2
13	4	1	4
14	4	2	3
15	4	3	2
16	4	4	1

Table S3. Range analysis of multiplying results.

NUMBER	FACTOR			Average value of multiplying data $\overline{X}$ (mAh·g^{-1})
	A Hydrothermal temperature (℃)	B Processing time (h)	C Carbon black raw material	
1	1	1	1	638.80
2	1	2	2	637.29
3	1	3	3	603.97
4	1	4	4	553.20
5	2	1	2	596.32
6	2	2	1	668.37
7	2	3	4	520.95
8	2	4	3	590.59
9	3	1	3	567.73
10	3	2	4	649.18
11	3	3	1	452.50
12	3	4	2	293.02
13	4	1	4	519.85
14	4	2	3	528.70
15	4	3	2	470.71
16	4	4	1	404.07
K_1	2433.26	2322.70	2163.74	
K_2	2376.23	2483.55	1997.34	
K_3	1962.43	2048.12	2290.99	
K_4	1923.33	1840.88	2243.18	
$k_1=K_1/4$	608.31	580.67	540.93	
$k_2=K_2/4$	594.06	620.89	499.34	
$k_3=K_3/4$	490.61	512.03	572.75	
$k_4=K_4/4$	480.83	460.22	560.80	
R	127.48	160.67	73.41	

Table S4. Variance analysis of multiplying results.

SOURCE	Type III Sum of Squares(*SS*)	*df*	Mean Square(*MS*)	*F*	*Sig.*
Hydrothermal temperature	53927.473	3	17975.824	4.595	0.054
Processing time	61184.688	3	20394.896	5.213	0.041
Carbon black raw material	12446.604	3	4148.868	1.061	0.433
Error	23473.062	6	3912.177		
Corrected Total	151031.827	15			

Table S5. Range analysis of cycle results.

NUMBER	FACTOR			Specific Capacity (0.5 C, 100 cycles, $mAh \cdot g^{-1}$)
	A Hydrothermal temperature (℃)	B Processing time (h)	C Carbon black raw material	
1	1	1	1	588.20
2	1	2	2	723.43
3	1	3	3	614.27
4	1	4	4	704.60
5	2	1	2	564.05
6	2	2	1	600.00
7	2	3	4	495.94
8	2	4	3	552.02
9	3	1	3	689.85
10	3	2	4	600.22
11	3	3	1	437.88
12	3	4	2	484.43
13	4	1	4	601.41
14	4	2	3	613.43
15	4	3	2	475.21
16	4	4	1	435.31
K_1	2630.50	2443.52	2061.38	
K_2	2212.01	2537.08	2247.11	
K_3	2212.37	2023.29	2469.57	
K_4	2125.36	2176.35	2402.18	
$k_1=K_1/4$	657.62	610.88	515.35	
$k_2=K_2/4$	553.00	634.27	561.78	
$k_3=K_3/4$	553.09	505.82	617.39	
$k_4=K_4/4$	531.34	544.09	600.54	
R	126.28	128.45	102.05	

Table S6. Variance analysis of cycle results.

SOURCE	Type III Sum of Squares(*SS*)	*df*	Mean Square(*MS*)	*F*	*Sig.*
Hydrothermal temperature	38762.690	3	12920.897	5.199	0.042
Processing time	42139.822	3	14046.607	5.651	0.035
Carbon black raw material	24707.794	3	8235.931	3.314	0.099
Error	14912.847	6	2485.475		
Corrected Total	120523.154	15			

Table S7. Comparison of electrochemical performance of some carbonaceous cathodes.

Cathode Material	**S content of the composite (%)**	**Voltage range (V)**	**Current density**	**Capacity ($mAh \cdot g^{-1}$)/Cycle Number**	**Capacity Decay Rate (%)**	**Ref.**
OPAB-140-1.5@S	75	1.7-2.8	0.2 C	602/400	0.08	This work
$S/SiO_2/CB$	70	1.5-3.0	0.1 C	736/50	0.76	S1
Cellulose(CMK-3/S)CB	45	1.5-2.8	0.5 C	660/300	0.12	S2
S@CN@OCN	57	1.6-2.5	1.0 C	-/400	0.06	S3
S/GN–CNT	76.4	1.7-2.8	0.5 C	463.7/500	0.08	S4
COB(0.1)-40/S	60	1.7-3.0	0.5 C	400.86/610	~0.10	S5
S/ONPC	47.6	1.0-3.0	0.2 C	613/100	0.47	S6
S/porous carbon	70	1.7-2.8	0.5 C	450/200	0.32	S7
HKC-S	55	1.5-3.0	0.2 C	607.7/300	0.16	S8
PEDOT-CMK-3/S	44.4	1.5-2.8	0.1 C	600/100	0.39	S9
Activated-carbon/sulfur	49.4	1.7-2.8	0.1 C	576/100	0.59	S10
Shaddock wadding carbon -sulfur	73.7	1.7-2.8	0.2 C	599/200	0.21	S11

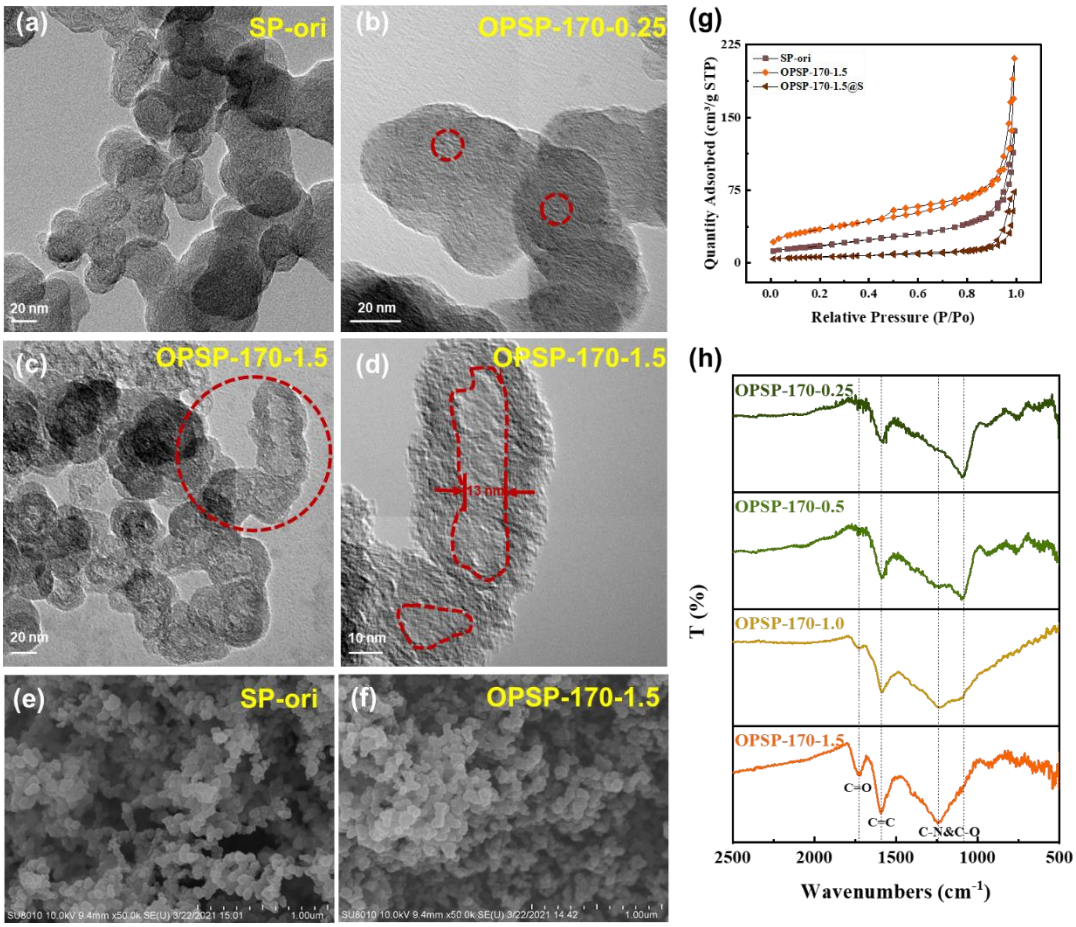

Figure S1. Physical characterization of SP-ori and OPSPs. TEM images of (a) SP-ori, (b) OPSP-170-0.25, (c-d) OPSP-170-1.5; SEM images of (e) SP-ori and (f) OPSP-170-1.5; (g) N_2 adsorption-desorption isotherms of SP-ori, OPSP-170-1.5 and OPSP-170-1.5@S; (h) FTIR spectra of OPSP-170-n (n=0.25, 0.5, 1.0, 1.5).

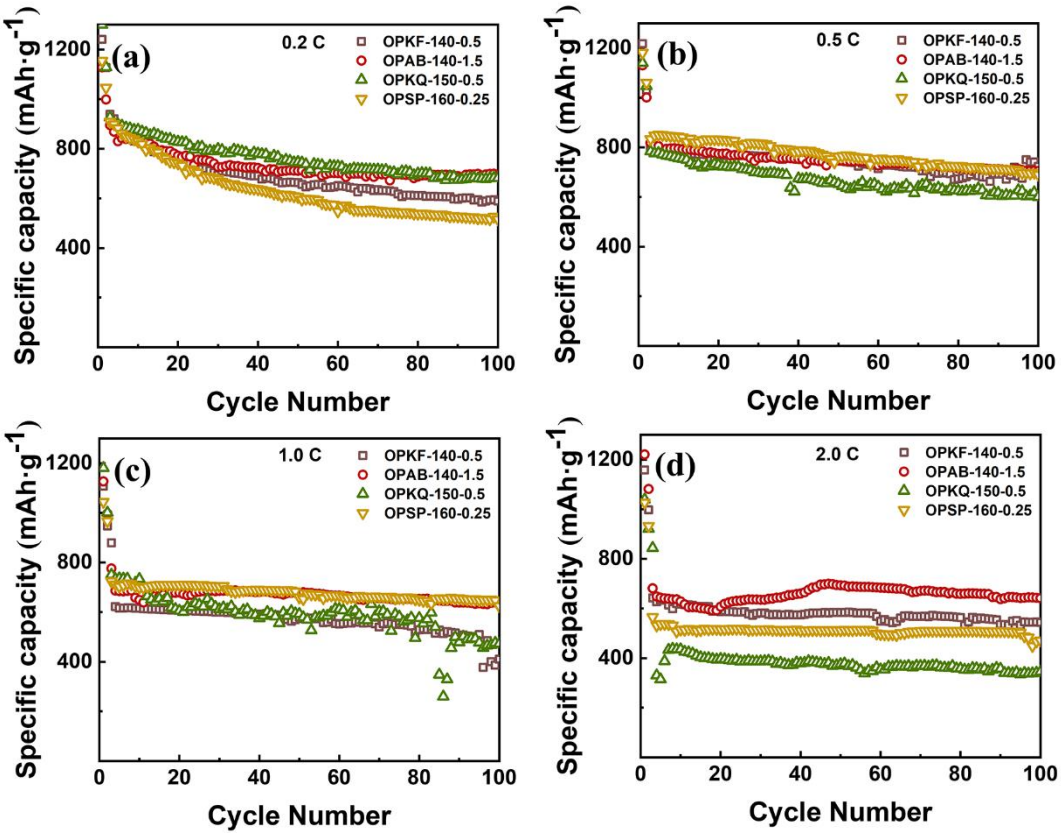

Figure S2. Comprehensive cycle tests of four representative materials. Comparison of cycling performances of four materials at the current rate of (a) 0.2 C, (b) 0.5 C, (c) 1.0 C, (d) 2.0 C.

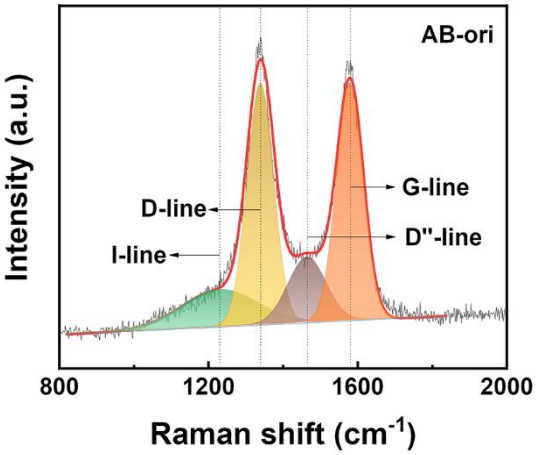

Figure S3. 4-peak model fitting result of AB-ori.

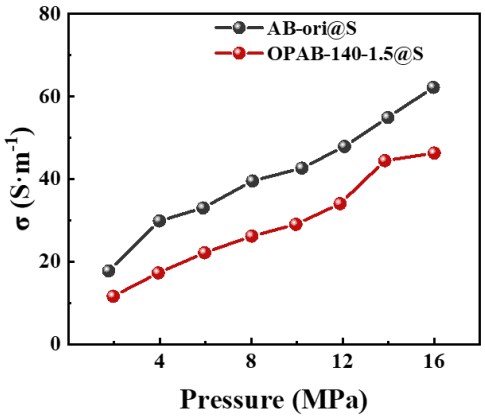

Figure S4. The conductivity comparation of AB-ori@S and OPAB-140-1.5@S.

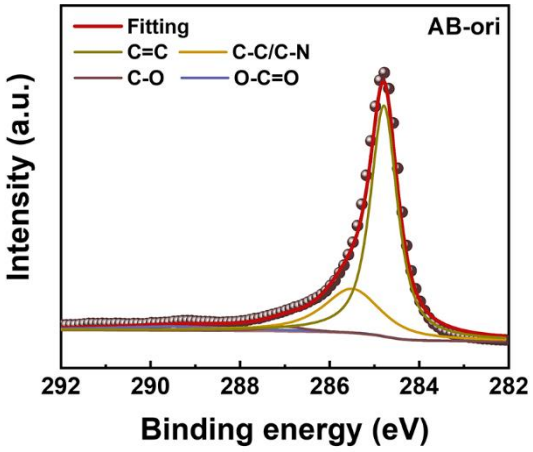

Figure S5. XPS C1s spectrum of AB-ori.

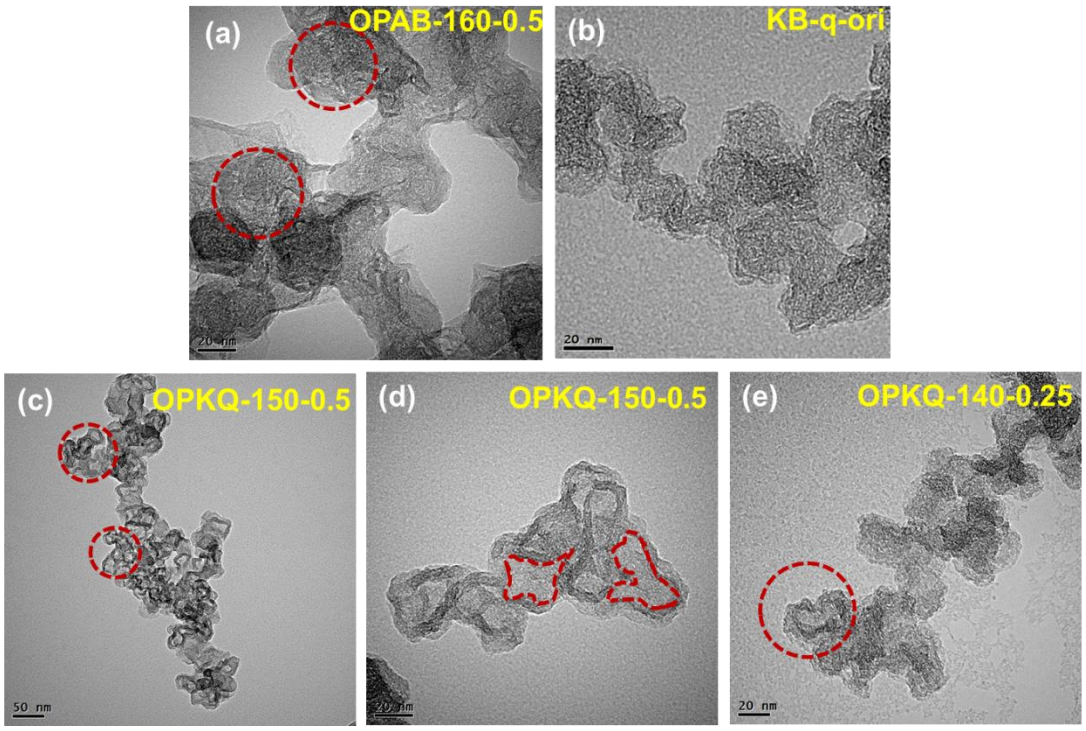

Figure S6. TEM images of (a) OPAB-160-0.5, (b) KB-q-ori, (c) OPKQ-150-0.5, (d) OPKQ-150-0.5, (e) OPKQ-140-0.25.

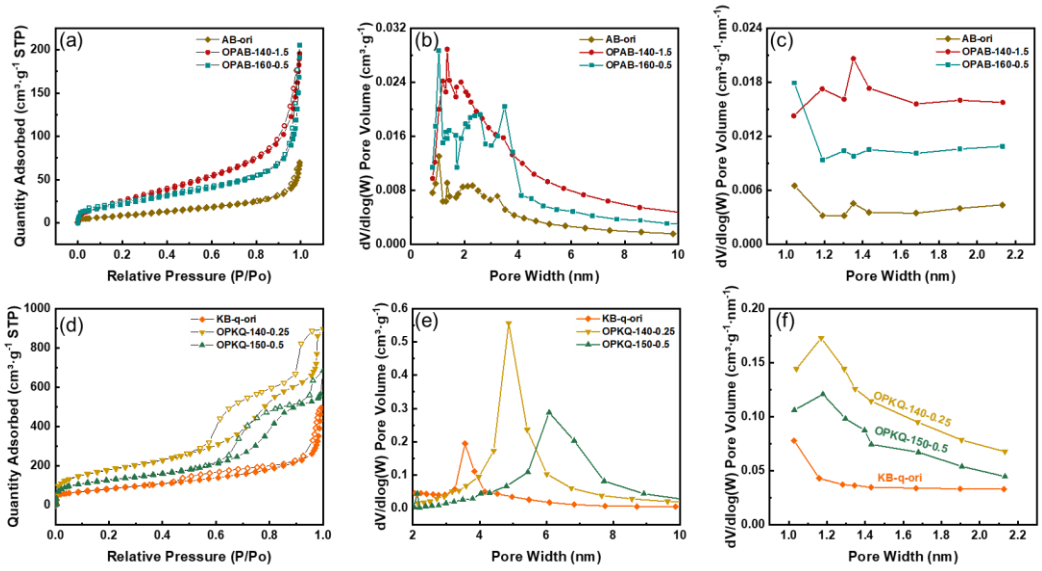

Figure S7. Characterization of pore structure of several representative OPCB materials. (a) N_2 adsorption-desorption isotherms, (b) pore-size distribution by NLDFT method and (c) micropore-size distribution based on H-K model of AB-ori, OPAB-140-1.5 and OPAB-160-0.5; (d) N_2 adsorption-desorption isotherms, (e) pore-size distribution by NLDFT method and (f) micropore-size distribution based on H-K model of KB-q-ori, OPKQ-140-0.25 and OPKQ-150-0.5.

Based on the above observations and Figure S1(OPSP), it is conjectured that there is a critical condition for the formation of hollow-characteristic structure, which is related to the raw materials. And when the hydrothermal parameters are adjusted below the critical value, only the evolution of the number of pores and the small change of the size occur. By comparing the specific surface area of Super P and KB-q-ori and their hydrothermal conditions with obvious hollow-like structure, we find that the critical condition is easier to achieve for raw carbon black materials with larger surface area.

To further examine effects of temperature and processing time on pores, nitrogen

adsorption and desorption experiments are conducted at 77 K (Figure S7). The hysteresis loop (especially materials made from KB-q) at high relative pressure manifests the appearance of mesopores. Evidently, the OPAB-140-1.5 which possessed a small peak at 1.35 nm exhibits a more remarkably rising PSD of micropores ($d < 2$ nm) than OPAB-160-0.5 which owns a peak at 3.50 nm within the scope of mesoporous. With reference to their respective preparation conditions, even extending the processing time at lower reaction temperature could not effectively enlarged pore size accompanied by the increase of the amount of pores merely, whereas raising the oxidation temperature has a more significant effect on expanding pore size. The comparative study of pore structures between OPKQ-140-0.25 annd OPKQ-150-0.5 are also carried out and the conjecture that increasing hydrothermal temperature plays a more effectual role to expand the aperture is confirmed by the fact that a peak at 6.08 nm appears in the PSD of OPKQ-150-0.5.

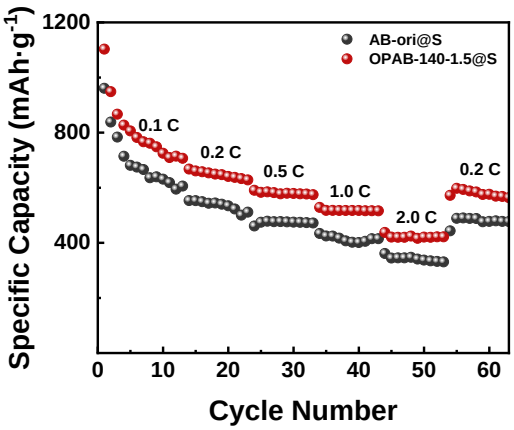

Figure S8. Rate capability of OPAB-140-1.5@S and AB-ori@S.

References

S1 P. Rajkumar, K. Diwakar, G. Radhika, K. Krishnaveni, R. Subadevi and M. Sivakumar, *Vacuum*, 2019, 161, 37-48.

S2 L. Li, L. Hou, J. Cheng, T. Simmons, F. Zhang, L. T. Zhang, R. J. Linhardt and N. Koratkar, *Energy Storage Mater.*, 2018, 15, 388-395.

S3 P. Chiochan, N. Phattharasupakun, J. Wutthiprom, M. Suksomboon, S. Kaewruang, P. Suktha and M. Sawangphruk, *Electrochim. Acta*, 2017, 237, 78-86.

S4 Z. Zhang, L. L. Kong, S. Liu, G. R. Li and X. P. Gao, *Adv. Energy Mater.*, 2017, 7, 1602543.

S5 W. W. Jin, J. Z. Zou, S. Z. Zeng, S. Inguva, G. Z. Xu, X. H. Li, M. Peng and X. R. Zeng, *Appl. Surf. Sci.*, 2019, 469, 404-413.

S6 Y. Zhao, L. Wang, L. Huang, M. Y. Maximov, M. Jin, Y. Zhang, X. Wang and G. Zhou, *Nanomaterials (Basel)*, 2017, 7, 402.

S7 Y. Zhu, G. Xu, X. Zhang, S. Wang, C. Li and G. Wang, *J. Alloys Compd.*, 2017, 695, 2246-2252.

S8 S. Leng, C. Chen, J. Liu, S. Wang, J. Yang, S. Shan, F. Gong, Y. Guo and M. Wu, *Appl. Surf. Sci.*, 2019, 487, 784-792.

S9 J. Song, H. Noh, J. Lee, I. W. Nah, W. I. Cho and H. T. Kim, *J. Power Sources*, 2016, 332, 72-78.

S10 S. Li, Z. Lin, G. He and J. Huang, *Colloid. Surface. A*., 2020, 602, 125129.

S11 W. Zhang, Y. Huang, X. Chen, H. Wu and X. Zhang, *J. Alloys Compd.*, 2017, 724, 575-580.